Interpretation of positron-annihilation data with respect to the electron-positron enhancement factors. II. Applications

G. Kontrym-Sznajd and A. Rubaszek
W. Trzebiatowski Institute of Low Temperature and Structure Research, Polish Academy of Sciences, P.O. Box 937, 50-950 Wrocław 2, Poland
(Received 31 August 1992)

The theoretical considerations of the properties of positron-annihilation characteristics in simple metals, presented in the previous paper, are verified for the alkali metals and Mg. Results are based on a local-density approach to electron-positron correlations and band-structure calculations are performed within the linear-muffin-tin-orbitals–average-spheres approximation. The validity of the average electron density approximation is discussed and the effective densities, determined by electron-positron correlation effects, are presented for valence electrons in simple metals. Methods of extracting the full shape of the electron-positron momentum density from experimental curves are recommended. The proposed analysis of experimental data applied to simple metals allows more reliable verificaton of the shape of electron-positron enhancement factors near the Fermi surface.

I. INTRODUCTION

In the interpretation of experimental data for angular correlation of positron-annihilation radiation (ACPAR) with respect to the electronic structure of materials, the knowledge of the electron-positron momentum-dependent enhancement factors $\varepsilon(\mathbf{p})$ is necessary. In Ref. 1 (hereafter referred to as I) properties of these parameters are discussed on mathematical grounds. In Sec. III our general considerations concerning valence electrons in simple metals are checked on the examples of alkali metals and Mg. Calculations are based on the band-structure results obtained within the linear-muffin-tin orbitals (LMTO)–average-spheres approximation (ASA). Electron-positron correlations are treated within the local-density approach (LDA).[2]

In I it was shown that the form of the positron wave function; the state-independent local electron-positron correlations; or, generally any state-independent correlations, slowly varying and periodic in the lattice function cannot change remarkably the shape of momentum density of valence electrons inside the central Fermi surface (FS) in simple metals. If the state-dependent correlations are applied within the LDA, the results for the electron-positron enhancement factors $\varepsilon_s^{\rm corr}(\mathbf{p})$ are very close to corresponding characteristics obtained by the average electron density[3,4] (AED) approximation.

The applicability of the AED for nearly free electronic (NFE) populations has an essential meaning. The LDA has been quite often applied[4] recently in calculations of positron-annihilation characteristics in real metals. Nevertheless, there is a question of which alternative electron-gas theories[4] provide correct enhancement factors $\varepsilon_{\rm jell}^{\rm corr}(p,r_s)$. Before applying the jellium results to LDA calculations in more complicated metals, we should verify $\varepsilon_{\rm jell}^{\rm corr}(p,r_s)$. The conversion LDA$\rightarrow$AED for momenta inside the FS gives such opportunity in the case of simple metals. The AED parameters $r_s^{\rm corr}$ for valence electrons in a few simple metals are presented in Sec. IV.

Another problem, connected with "experimental" enhancement factors $\varepsilon_{\rm expt}^{\rm corr}(\mathbf{p})$, follows from the fact that the biparabolic approximation of $\varepsilon^{\rm corr}(\mathbf{p})$, applied to fitting experimental ACPAR data,[5–8] is not valid even in an electron gas.[9] For this reason, the extraction of a real momentum dependence of $\varepsilon_{\rm expt}^{\rm corr}(\mathbf{p})$ is of vital interest. Section V is devoted to methods of working with experimental positron-annihilation data with respect to this problem.

II. BASIC FORMULAS

Here the main denotations used in I are briefly repeated. Electron momentum density (EMD) and 2γ momentum density of annihilation pairs are given by the expressions

$$\rho^e(\mathbf{p})=\frac{\pi r_0^2 c}{8\pi^3}\sum_{\mathbf{k}j} n(\mathbf{k}j)\left|\int e^{-i\mathbf{p}\cdot\mathbf{r}}\psi_{\mathbf{k}j}^e(\mathbf{r})d\mathbf{r}\right|^2 \tag{1}$$

and

$$\rho^{2\gamma}(\mathbf{p})=\frac{\pi r_0^2}{8\pi^3}\sum_{\mathbf{k}j} n(\mathbf{k}j)\left|\int e^{-i\mathbf{p}\cdot\mathbf{r}}\psi_{\mathbf{k}j}^{ep}(\mathbf{r},\mathbf{r})d\mathbf{r}\right|^2, \tag{2}$$

respectively. Here

$$\psi_{\mathbf{k}j}^e(\mathbf{r})=e^{i\mathbf{k}\cdot\mathbf{r}}\sum_{\mathbf{G}} u_{\mathbf{k}j}(\mathbf{G})e^{i\mathbf{G}\cdot\mathbf{r}} \tag{3}$$

are the electron wave functions in the host material, $\psi_{\mathbf{k}j}^{ep}(\mathbf{r}_e,\mathbf{r}_p)$ denote the pair wave functions of electron in the initial state $\mathbf{k}j$ at $\mathbf{r}_e$ and thermalized positron at $\mathbf{r}_p$, $n(\mathbf{k}j)$ are the occupation numbers of the states $\mathbf{k}j$, while r_0 and c are the classical electron radius and velocity of light, respectively. Momenta $\mathbf{p}$ in the Eqs. (1)–(3) are in the extended zone scheme and $\mathbf{k}$ are considered inside the first Brillouin zone (1BZ). Vectors $\mathbf{G}$ denote reciprocal lattice vectors. The total annihilation rate λ ($\lambda=1/\tau$, where τ is the positron lifetime) is related to $\rho^{2\gamma}(\mathbf{p})$ according to the expression

$$\lambda=\int \rho^{2\gamma}(\mathbf{p})d\mathbf{p}=\pi r_0^2 c \int d\mathbf{r} \sum_{\mathbf{k}j} n(\mathbf{k}j)|\psi_{\mathbf{k}j}^{ep}(\mathbf{r},\mathbf{r})|^2 . \quad (4)$$

Functions $\psi_{\mathbf{k}j}^{ep}(\mathbf{r},\mathbf{r})$ may be generally written as

$$\psi_{\mathbf{k}j}^{ep}(\mathbf{r},\mathbf{r})=\chi_{\mathbf{k}j}(\mathbf{r})\psi_{\mathbf{k}j}^{e}(\mathbf{r})=[f_{\mathbf{k}j}(\mathbf{r})]^{1/2}\psi_{+}(\mathbf{r})\psi_{\mathbf{k}j}^{e}(\mathbf{r}) , \quad (5)$$

where $\psi^{+}(\mathbf{r})$ stands for a positron wave function and $\chi_{\mathbf{k}j}(\mathbf{r})$ are periodic in the lattice, i.e.,

$$\chi_{\mathbf{k}j}(\mathbf{r})=\sum_{\mathbf{G}} h_{\mathbf{k}j}(\mathbf{G})e^{i\mathbf{G}\cdot\mathbf{r}} . \quad (6)$$

Depending on the approximation applied to $\psi_{\mathbf{k}j}^{ep}(\mathbf{r}_e,\mathbf{r}_p)$ we can distinguish the following cases.[1]

(i) The independent particle model (IPM), which assumes $f_{\mathbf{k}j}(\mathbf{r})=1$, i.e., $\chi_{\mathbf{k}j}(\mathbf{r})=\psi_{+}(\mathbf{r})$. Here we have

$$\rho^{\mathrm{IPM}}(\mathbf{p})=\varepsilon^{\mathrm{IPM}}(\mathbf{p})\times\rho^{e}(\mathbf{p}) .$$

(ii) The AED,[3,4] which corresponds to the LDA in a homogeneous system. In this case

$$f_{\mathbf{k}j}(\mathbf{r})=\varepsilon_{\mathrm{jell}}^{\mathrm{corr}}(\mathbf{k}j,r_s^{\mathrm{corr}}) ,$$

$$\chi_{\mathbf{k}j}(\mathbf{r})=\psi_{+}(\mathbf{r})[\varepsilon_{\mathrm{jell}}^{\mathrm{corr}}(\mathbf{k}j,r_s^{\mathrm{corr}})]^{1/2} ,$$

while

$$\rho^{\mathrm{AED}}(\mathbf{p})=\varepsilon_{\mathrm{jell}}^{\mathrm{corr}}(p,r_s^{\mathrm{corr}})\times\rho^{\mathrm{IPM}}(\mathbf{p}) .$$

(iii) The LDA employing state-independent correlations,[4] i.e.,

$$f_{\mathbf{k}j}(\mathbf{r})=\varepsilon_{\mathrm{jell}}^{\mathrm{corr}}[p_0,r_s(\mathbf{r})] ,$$

$$\chi_{\mathbf{k}j}(\mathbf{r})=\psi_{+}(\mathbf{r})\{\varepsilon_{\mathrm{jell}}^{\mathrm{corr}}[p_0,r_s(\mathbf{r})]\}^{1/2} ,$$

where momentum p_0 is independent of the state $\mathbf{k}j$ and its choice depends on the approach.[10] Here

$$\rho_0^{\mathrm{LDA}}(\mathbf{p})=\varepsilon_0^{\mathrm{corr}}(\mathbf{p})\times\rho^{\mathrm{IPM}}(\mathbf{p})=\varepsilon_0^{2\gamma}(\mathbf{p})\times\rho^{e}(\mathbf{p}) ,$$

where

$$\varepsilon_0^{2\gamma}(\mathbf{p})=\varepsilon_0^{\mathrm{corr}}(\mathbf{p})\times\varepsilon^{\mathrm{IPM}}(\mathbf{p}) .$$

(iv) The LDA using energy-dependent correlations, e.g.,

$$f_{\mathbf{k}j}(\mathbf{r})=\varepsilon_{\mathrm{jell}}^{\mathrm{corr}}[E_{\mathbf{k}j}/E_F,r_s(\mathbf{r})] ,$$

$$\chi_{\mathbf{k}j}(\mathbf{r})=\psi_{+}(\mathbf{r})\{\varepsilon_{\mathrm{jell}}^{\mathrm{corr}}[E_{\mathbf{k}j}/E_F,r_s(\mathbf{r})]\}^{2} ,$$

where $E_{\mathbf{k}j}$ and E_F are the energy of the state $\mathbf{k}j$ and Fermi energy, respectively. The corresponding momentum density is given by

$$\rho_s^{\mathrm{LDA}}(\mathbf{p})=\varepsilon_s^{\mathrm{corr}}(\mathbf{p})\times\rho^{\mathrm{IPM}}(\mathbf{p})=\varepsilon_s^{2\gamma}(\mathbf{p})\times\rho^{e}(\mathbf{p}) ,$$

where

$$\varepsilon_s^{2\gamma}(\mathbf{p})=\varepsilon_s^{\mathrm{corr}}(\mathbf{p})\times\varepsilon^{\mathrm{IPM}}(\mathbf{p}) .$$

(v) An exact form of $\psi_{\mathbf{k}j}^{ep}(\mathbf{r},\mathbf{r})$ which, according to our knowledge, has not been determined by theory up to now.

Equations (2), (3), (5), and (6) lead to the following expressions for the $\rho^{e}(\mathbf{p})$ and the "generalized" momentum density $\rho(\mathbf{p})$ (for more details see I):

$$\rho^{e}(\mathbf{p}=\mathbf{k}+\mathbf{G}^*)=\sum_{\mathbf{k}j} n(\mathbf{k}j)|u_{\mathbf{k}j}(\mathbf{G}^*)|^2 \quad (7)$$

and

$$\rho(\mathbf{p}-\mathbf{k}+\mathbf{G}^*)=|u_{\mathbf{k}j^*}(\mathbf{G}^*)|^2|h_{\mathbf{k}j^*}(\mathbf{0})|^2 \times|1+\alpha(\mathbf{k}j^*,\mathbf{G}^*)|^2 \times\left[n(\mathbf{k}j^*)+\sum_{j\neq j^*}|\beta(\mathbf{k}j,\mathbf{G}^*)|^2\right] , \quad (8a)$$

respectively, where

$$\alpha(\mathbf{k}j,\mathbf{G}^*)=[h_{\mathbf{k}j}(\mathbf{G}^*-\mathbf{G}_{\mathbf{k}j})]^{-1} \times\sum_{\mathbf{G}\neq\mathbf{G}_{\mathbf{k}j}} h_{\mathbf{k}j}(\mathbf{G}-\mathbf{G}^*)u_{\mathbf{k}j}(\mathbf{G})/u_{\mathbf{k}j}(\mathbf{G}_{\mathbf{k}j}) \quad (8b)$$

and

$$\beta(\mathbf{k}j,\mathbf{G}^*)=n(\mathbf{k}j)\frac{h_{\mathbf{k}j}(\mathbf{G}^*-\mathbf{G}_{\mathbf{k}j})}{h_{\mathbf{k}j}(\mathbf{0})}\frac{u_{\mathbf{k}j}(\mathbf{G}_{\mathbf{k}j})}{u_{\mathbf{k}j^*}(\mathbf{G}^*)}\frac{h_{\mathbf{k}j}(\mathbf{0})}{h_{\mathbf{k}j^*}(\mathbf{0})} \times\frac{[1+\alpha(\mathbf{k}j,\mathbf{G}^*)]}{[1+\alpha(\mathbf{k}j^*,\mathbf{G}^*)]} . \quad (8c)$$

Vectors $\mathbf{G}_{\mathbf{k}j}$ and band j^* fulfill the relations

$$|u_{\mathbf{k}j}(\mathbf{G}_{\mathbf{k}j})|\geq|u_{\mathbf{k}j}(\mathbf{G})| \quad \text{for } \mathbf{G}\neq\mathbf{G}_{\mathbf{k}j} ,$$

$$|u_{\mathbf{k}j^*}(\mathbf{G}^*)|\geq|u_{\mathbf{k}j}(\mathbf{G}^*)| \quad \text{for } j\neq j^* ,$$

$$\mathbf{G}_{\mathbf{k}j^*}=\mathbf{G}^* .$$

III. INFLUENCE OF POSITRON DISTRIBUTION AND STATE-INDEPENDENT CORRELATIONS ON THE RESULTING ACPAR SPECTRUM

In this section we examine models (i) and (iii) of Sec. II [which assume $\chi_{\mathbf{k}j}(\mathbf{r})$ independent of the electronic state $\mathbf{k}j$] in few representatives of simple metals. Results, based on LMTO-ASA band-structure calculations,[11] confirm our theoretical considerations presented in I.

Valence electrons in simple metals are described by the NFE model reasonably well. Except for the states $\mathbf{k}j$ close to the BZ boundary, within the NFE and for momenta $\mathbf{p}$ inside the central FS there is only one "leading" Fourier coefficient in the expansion (3) of $\psi_{\mathbf{k}j}^{e}(\mathbf{r})$ [namely, $u_{\mathbf{k}j}(\mathbf{G}_{\mathbf{k}j})$], and the other (umklapp) components are very small. Due to this fact the momentum-dependent functions $\alpha(\mathbf{k}j,\mathbf{G}^*)$ and $\beta(\mathbf{k}j,\mathbf{G}^*)$ in Eqs. (8) are almost negligible and the resulting enhancement factor $\varepsilon(\mathbf{p}=\mathbf{k}+\mathbf{G}^*)=\rho(\mathbf{p})/\rho^{e}(\mathbf{p})$ is close to $|h_{\mathbf{k}j^*}(\mathbf{0})|^2$. Thus, in the case of the IPM or state-independent correlation functions the nearly constant value of $\varepsilon(\mathbf{p})$ should be obtained. The aim of this section is to verify this hypothesis in a series of simple metals.

In alkali metals the Fermi momentum is inside the 1BZ and only one band $j^*=1$ is occupied, i.e., $\beta(\mathbf{k}j,\mathbf{G}^*)=0$ for $j\neq1$. For momenta $\mathbf{p}$ inside the FS we have

$$\varepsilon(\mathbf{p}=\mathbf{k})=|h(\mathbf{0})|^2|1+\alpha(\mathbf{k}1,\mathbf{0})|^2 .$$

It is apparent that if $\chi(\mathbf{r})$ is not state selective, the function $\alpha(\mathbf{k}1,\mathbf{0})$ is the only one responsible for momentum dependence of $\varepsilon(\mathbf{p})$. It is obvious that $|\alpha(\mathbf{k}1,\mathbf{0})|$ achieves its maximum at the FS, since $|u_{\mathbf{k}1}(\mathbf{0})|$ decreases when $\mathbf{k}$ approaches the BZ boundary [while the umklapp components $u_{\mathbf{k}1}(\mathbf{G}\neq\mathbf{0})$ increase]. The values of

$$\varepsilon^{\mathrm{IPM}}(\mathbf{p})/\varepsilon^{\mathrm{IPM}}(\mathbf{0})=|1+\alpha^{\mathrm{IPM}}(\mathbf{k}1,\mathbf{0})|^2$$

in Li, Na, K, and Mg for $\mathbf{p}=\mathbf{p}_F$ are displayed in the second row of Table I. It can be seen that values of $|\alpha^{\mathrm{IPM}}(\mathbf{p}_F 1,\mathbf{0})|$ do not exceed 2%. That confirms our calculations of I and is consistent with results obtained by Sormann.[12] The change in $\varepsilon_0^{\mathrm{corr}}(\mathbf{p})=\varepsilon_0^{2\gamma}(\mathbf{p})/\varepsilon^{\mathrm{IPM}}(\mathbf{p})$ at the FS is even less pronounced (up to 1%), as $\varepsilon_0^{\mathrm{corr}}[0,r_s(\mathbf{r})]$ is more slowly varying function than $\psi_+(\mathbf{r})$, especially in the vicinity of the ionic cores (the same conclusions are valid in Mg, as shown below).

In Mg the Fermi momentum $\mathbf{p}_F$ is outside the 1BZ. This is illustrated in Fig. 1, where the spherical FS of hexagonal close-packed metal with two s electrons per atom is shown both in the extended ($\mathbf{p}$ space) and the reduced ($\mathbf{k}$ space) zone schemes. It can be seen that in the second band ($j=2$) the leading term in the expansion (3) of the electron wave function is $u_{\mathbf{k}2}(\mathbf{G}_1)$ (where $\mathbf{G}_1=[100]$) for momenta $\mathbf{k}$ inside the area ΣLM, and $u_{\mathbf{k}2}(-[001])$ for $\mathbf{k}$ inside the area $\Gamma AL\Sigma$. If $\mathbf{p}=\mathbf{k}+\mathbf{G}_1$ is above the line ΣL, the band $j^*=3$ gives the main contribution to $\rho^e(\mathbf{p})$ and $\rho(\mathbf{p})$. So, within NFE, for momenta $\mathbf{p}=\mathbf{k}+\mathbf{G}^*$ inside the FS (except the states on the BZ boundary) the contribution of only one state $\mathbf{k}j^*$ dominates in $\rho^e(\mathbf{p})$, i.e., $\rho^e_{\mathrm{NFE}}(\mathbf{p}=\mathbf{k}+\mathbf{G}^*)\cong|u_{\mathbf{k}j^*}(\mathbf{G}^*)|^2$.

Let us consider momenta $\mathbf{p}=(p_x,0,0)$ along the line ΓM. Inside the 1BZ $\rho^e_{\mathrm{NFE}}(\mathbf{p})$ reads as

$$\rho^e_{\mathrm{NFE}}(\mathbf{p}=\mathbf{k})\cong n(\mathbf{k}1)|u_{\mathbf{k}1}(\mathbf{0})|^2 \quad \text{for } \mathbf{k}\in\Gamma AL\Sigma \text{ (or } |p|\leq|\Gamma M|)\,. \tag{9a}$$

Outside the 1BZ we have

$$\rho^e_{\mathrm{NFE}}(\mathbf{p}=\mathbf{k}+\mathbf{G}_1)\cong n(k2)|u_{\mathbf{k}2}(\mathbf{G}_1)|^2 \quad \text{for } k\in\Sigma LM \text{ (or } |\Gamma M|\leq|\mathbf{p}|\leq|\mathbf{p}_F|)\,. \tag{9b}$$

In the case of Fermi momentum outside the 1BZ, both the terms $\alpha(\mathbf{k}j,\mathbf{G}^*)$ and $\beta(\mathbf{k}j,\mathbf{G}^*)$ appear in Eqs. (8). In particular, due to nonzero values of $\beta(\mathbf{k}j,\mathbf{G}^*)$, the jumps in $\rho^{\mathrm{IPM}}(\mathbf{p})$ and $\rho_0^{\mathrm{LDA}}(\mathbf{p})$ should be observed in the region of the band superposition. Nevertheless, our calculations of $\rho^{2\gamma}(\mathbf{p})$ in Mg (Ref. 11(c)] indicate that these jumps are very small, as predicted on mathematical grounds in I. Within the IPM the results for the enhancement factor $\varepsilon^{\mathrm{IPM}}(\mathbf{p})$ are as follows: $\varepsilon^{\mathrm{IPM}}(\mathbf{p})/\varepsilon^{\mathrm{IPM}}(\mathbf{0})=1$, 1.002, and 1.042 for $|\mathbf{p}|\leq|\mathbf{p}_2|$, $|\mathbf{p}_2|\leq|\mathbf{p}|\leq|\Gamma M|$, and $|\Gamma M|\leq|\mathbf{p}|\leq|\mathbf{p}_F|$, respectively (see Fig. 1). If state-independent local correlations $\varepsilon^{\mathrm{corr}}_{\mathrm{jell}}[0,r_s(\mathbf{r})]$ are applied [model (iii) of Sec. II with $p_0=0$], the changes in $\varepsilon_0^{2\gamma}(\mathbf{p})/\varepsilon_0^{2\gamma}(\mathbf{0})$ are a bit more pronounced: they amount to 1.0, 1.002, and 1.052, respectively.

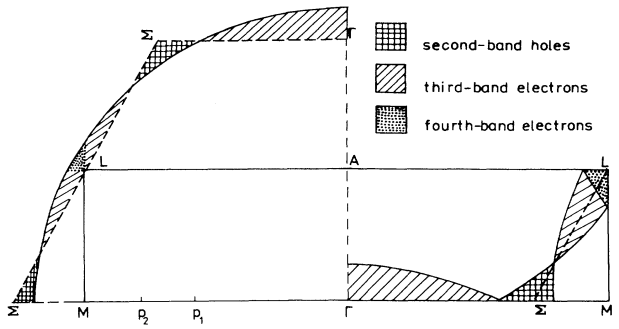

FIG. 1. Fermi surface of Mg on the ΓMLA plane in the extended (left-hand side) and reduced (right-hand side) zone schemes p_1 and p_2 mark the region where $\rho(\mathbf{p})=\rho_1(\mathbf{p})$, i.e., only one band is occupied.

This behavior of enhancement factors has been predicted by our theoretical considerations of I. Namely, if the small contribution of $\alpha(\mathbf{k}j,\mathbf{G}^*)$ in relation (8) is neglected (see the Appendix in I and results for alkali metals), $\rho^{\mathrm{IPM}}(\mathbf{p})$ and $\rho_0^{2\gamma}(\mathbf{p})$ may be approximated by

$$\rho_{\mathrm{NFE}}(\mathbf{p}=\mathbf{k}+\mathbf{G}^*)\cong|u_{\mathbf{k}j^*}(\mathbf{G}^*)|^2|h(\mathbf{0})|^2\times\left[n(\mathbf{k}j^*)+\sum_{j\neq j^*}|\beta(\mathbf{k}j,\mathbf{G}^*)|^2\right], \tag{10a}$$

where within the NFE

$$\beta(\mathbf{k}j,\mathbf{G}^*)\cong n(\mathbf{k},j)\frac{h(\mathbf{G}^*-\mathbf{G}_{\mathbf{k}j})}{h(\mathbf{0})}\frac{u_{\mathbf{k}j}(\mathbf{G}_{\mathbf{k}j})}{u_{\mathbf{k}j^*}(\mathbf{G}^*)}\,. \tag{10b}$$

Equations (9) and (10) lead to the following values of $\varepsilon(p)$ in Mg:

$$\varepsilon(\mathbf{p})=|h(\mathbf{0})|^2 \quad \text{for } |\mathbf{p}|\leq|\mathbf{p}_2|\,,$$

$$\varepsilon(\mathbf{p})=|h(\mathbf{0})|^2\left[1+\left|\frac{h(-\mathbf{G}_1)}{h(\mathbf{0})}\frac{u_{\mathbf{k},2}(\mathbf{G}_1)}{u_{\mathbf{k},1}(\mathbf{0})}\right|^2\right] \quad \text{for } |\mathbf{p}_2|\leq|\mathbf{p}|\leq|\Gamma M|\,,$$

TABLE I. Enhancement factors $\varepsilon^{\mathrm{IPM}}(\mathbf{p})/\varepsilon^{\mathrm{IPM}}(\mathbf{0})$ and $\varepsilon_0^{\mathrm{corr}}(\mathbf{p})/\varepsilon_0^{\mathrm{corr}}(\mathbf{0})$ at the FS in simple metals. Results are based on the LDA and band-structure calculations performed within LMTO-ASA (Ref. 11). $\rho_0^{\mathrm{LDA}}(\mathbf{p})$ and $\rho^e(\mathbf{p})$ are normalized to unity at $\mathbf{p}=\mathbf{0}$.

Metal	$\bar{\varepsilon}^{\mathrm{IPM}}(\mathbf{p}_F)$	$\bar{\varepsilon}_0^{\mathrm{corr}}(\mathbf{p}_F)$	$\bar{\rho}_0^{\mathrm{LDA}}(\mathbf{p}_F)$	$\bar{\rho}^e(p_F)$
Li [100]	0.9821	0.9926	0.9694	0.9949
[110]	0.9802	0.9915	0.7917	0.8150
Na [100]	1.0047	1.0040	0.9918	0.9847
[110]	1.0047	1.0030	0.9907	0.9829
K [100]	1.0117	1.0100	0.9803	0.9587
[110]	1.0027	1.0030	0.9299	0.9237
Mg [100]	1.0418	1.0100	0.9486	0.9015

$$\varepsilon(\mathbf{p})=|h(\mathbf{0})|^2\left[1+\left|\frac{h(\mathbf{G}_1)}{h(\mathbf{0})}\frac{u_{\mathbf{k},1}(\mathbf{0})}{u_{\mathbf{k},2}(\mathbf{G}_1)}\right|^2\right]$$

$$\text{for } |\Gamma M|\le|\mathbf{p}|\le|\mathbf{p}_F| \ .$$

However, $h(-\mathbf{G}_1)=h(\mathbf{G}_1)$ (since the lattice potential is real and has inversion symmetry) and a jump in $\varepsilon(\mathbf{p})$ at $|\mathbf{p}|=\Gamma M$ depends on the ratio $u_{\mathbf{k},2}(\mathbf{G}_1)/u_{\mathbf{k},1}(\mathbf{0})$ only. Since this ratio is less than unity, $\varepsilon(\mathbf{p})$ has higher values in the third region. This fact is in agreement with the LDA and LMTO-ASA results presented here.

The above results indicate that the positron distribution and state-independent electron-positron correlations have considerably less influence on the shape of $\rho^{2\gamma}(\mathbf{p})$ than the band effects [i.e., deviation of $u_{\mathbf{k}j}(\mathbf{G}_{\mathbf{k}j})$ from unity; see columns 4 and 5 of Table I] since the momentum distributions $\rho^{2\gamma}(\mathbf{p})$ is almost proportional to $\rho^e(\mathbf{p})$ in our case. Moreover, except for Li, at the FS $\rho^{2\gamma}(\mathbf{p})/\rho^{2\gamma}(\mathbf{0})$ is closer to unity that $\rho^e(\mathbf{p})/\rho^e(\mathbf{0})$. The fact that the positron distribution reduces the influence of the lattice potential on the resulting momentum density is in agreement with expectations. The IPM electron-positron wave function $\psi^{\mathrm{IPM}}_{\mathbf{k}j}(\mathbf{r}_e,\mathbf{r}_p)=\psi^e_{\mathbf{k}j}(\mathbf{r}_e)\psi_+(\mathbf{r}_p)$ is the eigenfunction of the Schrödinger equation (in Rydberg units)

$$[-\nabla_e^2-\nabla_P^2+V_+(\mathbf{r}_p)+V_-(\mathbf{r}_e)]\psi^e_{\mathbf{k}j}(\mathbf{r}_e)\psi_+(\mathbf{r}_P)$$
$$=(E_{\mathbf{k}j}+E_+)\psi^e_{\mathbf{k}j}(\mathbf{r}_e)\psi_+(\mathbf{r}_p) \ ,$$

where V_- and V_+ are the effective one-particle electron and positron potentials, respectively, and E_+ is a positron energy. For $\mathbf{r}_e=\mathbf{r}_p$ Coulomb parts of $V_-(\mathbf{r}_e=\mathbf{r}_p)$ and $V_+(\mathbf{r}_p)$ cancel each other and only the electron-electron exchange-correlation part of $V_-(\mathbf{r}_p)$ remains. As a result, the positron wave function $\psi_+(\mathbf{r})$ "smooths" the position dependence of the product $\psi^e_{\mathbf{k}j}(\mathbf{r}_e=\mathbf{r}_p)\psi(\mathbf{r}_p)$, especially inside the muffin-tin sphere, and dumps the lattice effects in $\rho^{\mathrm{IPM}}(\mathbf{p})$ with respect to $\rho^e(\mathbf{p})$. On the other hand, electron-positron correlations considered within the LDA are slowly varying functions of positron position $\mathbf{r}_p$ are at the high-density region (i.e., in the vicinity of the ionic core, where $\psi^e_{\mathbf{k}j}$ change rapidly) and therefore should not reproduce considerably the band effects in $\rho^{2\gamma}(\mathbf{p})$. This fact is illustrated in Fig. 2 where the momentum dependence of $\varepsilon^{2\gamma}(\mathbf{p})$ and $\rho^e(\mathbf{p})$ is shown. Let us point out that characteristics inside the FS are drawn in the scale enlarged 20 times in comparison to the one for high-momentum components (HMC). Expt for Li, $\varepsilon^{2\gamma}(\mathbf{p})$ behaves as $1/\rho^e(\mathbf{p})$: if $\rho^e(\mathbf{p})$ decreases, $\varepsilon^{2\gamma}(\mathbf{p})$ increases (see Table I and Fig. 2). This effect is observed both for momenta inside the FS and HMC. For umklapp components, however, the momentum dependence of $\varepsilon^{2\gamma}(\mathbf{p})$ is much more pronounced than in the central FS. This feature of $\varepsilon^{2\gamma}(\mathbf{p})$ for momenta $\mathbf{p}$ outside the FS is connected with strong momentum dependence of HMC of $\rho^e(\mathbf{p})$.

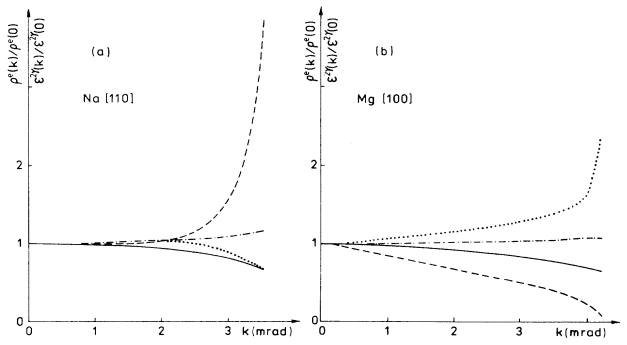

FIG. 2. Momentum dependence of $\varepsilon_1^{2\gamma}(\mathbf{p})$ and $\rho_1^e(\mathbf{p})$ in the first band as a function of $\mathbf{k}$. Characteristics $\rho^e(\mathbf{p})$ and $\varepsilon^{2\gamma}(\mathbf{p})$ inside the FS (the scale is enlarged 20 times) are shown by solid and dash-dotted curves, respectively. The HMC values of $\rho^e(\mathbf{p})$ and $\varepsilon^{2\gamma}(\mathbf{p})$ are marked by dashed and dotted lines, respectively. Results are based on LMTO-ASA and LDA (Ref. 11).

IV. APPLICABILITY OF AED IN SIMPLE METALS

As shown in I, for momenta $\mathbf{p}$ inside the FS, the enhancement factor reads as

$$\varepsilon^{\mathrm{corr}}(\mathbf{p}=\mathbf{k}+\mathbf{G}^*)=|h_{\mathbf{k}j^*}(\mathbf{0})|^2[1+\zeta(\mathbf{p})] \qquad (11)$$

where $\zeta(\mathbf{p})$ is a monotonic function of $\mathbf{p}$ inside the FS and achieves its extreme at $\mathbf{p}=\mathbf{p}_F$. This function is related to $\alpha(\mathbf{k}j,\mathbf{G}^*)$ and $\beta(\mathbf{k}j,\mathbf{G}^*)$ according to Eqs. (7) and (8). The form of $\zeta(\mathbf{p})$ depends mainly on the ratios of umklapp to main components of $\psi^e_{\mathbf{k}j}(\mathbf{r})$. For NFE populations $\alpha(\mathbf{k}j,\mathbf{G}^*)$ and $\beta(\mathbf{k}j,\mathbf{G}^*)$ are only small corrections (see Sec. III) and therefore the momentum dependence of $\zeta(\mathbf{p})$ inside the FS should be very weak. Within models (i) and (iii) of Sec. II, $[1+\zeta(\mathbf{p})]/[1+\zeta(\mathbf{0})]=\varepsilon^{\mathrm{corr}}(\mathbf{p})/\varepsilon^{\mathrm{corr}}(\mathbf{0})$. These values in a few simple metals are displayed in columns 2 and 3 of Table I (for IPM and for state-independent correlations $\varepsilon^{\mathrm{corr}}_{\mathrm{jell}}[0,r_s(\mathbf{r})]$, respectively). It can be seen that these quantities are very close to unity [$\zeta(\mathbf{p}_F)$ does not exceed 2%]. Since $\zeta(\mathbf{p})$ provides only small correction to $\varepsilon^{\mathrm{corr}}(\mathbf{p})$, the momentum dependence of the electron-positron enhancement factors inside the FS is due to the state selectivity of the two-particle correlation function $f_{\mathbf{k}j}(\mathbf{r})$ only. Neither the form of the positron wave function nor the state-independent correlations can change visibly the shape of $\rho^{2\gamma}(\mathbf{p})$ inside the FS with respect to $\rho^e(\mathbf{p})$ for delocalized electrons (e.g., valence electrons in simple metals).

In some cases Eq. (11) enables us to reduce LDA to AED, where the density of valence electrons is described by the effective electron density parameter r_s^{corr}. Applicability of AED in simple metals would be a great advantage in studies of the correlations effects in real solids. Namely, it would allow for verification of given electron-gas theory before applying it to calculation of annihilation characteristics in more complicated metals within the LDA.

If the LDA [model (iv) of Sec. II] is applied, Eq. (11) may be written in the AED form:[3]

$$\varepsilon^{\rm corr}_{\rm LDA}(\mathbf{p}=\mathbf{k}+\mathbf{G}^*)=\int \varepsilon^{\rm corr}_{\rm jell}[E_{\mathbf{k}j^*}/E_F, r_s(\mathbf{r})]|\psi_+(\mathbf{r})|^2 d\mathbf{r}[1+\zeta_{\rm LDA}(\mathbf{p})]$$
$$=\varepsilon^{\rm corr}_{\rm jell}[E_{\mathbf{k}j^*}/E_F, r_s(\mathbf{r}_P)][1+\zeta_{\rm LDA}(\mathbf{p})]\ . \quad (12)$$

Apart from coefficients $\alpha(\mathbf{k}j,\mathbf{G}^*)$ and $\beta(\mathbf{k}j,\mathbf{G}^*)$, $\zeta_{\rm LDA}(\mathbf{p})$ contains here also the correction $\sum|h_{\mathbf{k}j^*}(\mathbf{G})/h_{\mathbf{k}j^*}(\mathbf{0})|^2$, where the summation is performed over vectors $\mathbf{G}\neq\mathbf{0}$.

The conversion LDA$\rightarrow$AED for momenta $\mathbf{p}$ inside the FS is reliable if (i) te first term in (12) leads for all momenta $\mathbf{p}$ to the same value of $r_s(\mathbf{r}_p)=r_s^{\rm corr}$ (see discussion in I) and (ii) $[1+\zeta(\mathbf{p})]$ is a known small correction independent of the choice of the electron-gas theory providing $\varepsilon^{\rm corr}_{\rm jell}(\mathbf{p},r_s)$.

With respect to the condition (ii), $\zeta_{\rm LDA}(\mathbf{p})$ depends only on the electronic structure of material [providing values of $u_{\mathbf{k}j}(\mathbf{G})/u_{\mathbf{k}j}(\mathbf{G}_{\mathbf{k}j})$] and the ratios $h_{\mathbf{k}j}(\mathbf{G})/h_{\mathbf{k}j}(\mathbf{0})$, i.e. on the degree of localization of electrons and lattice potential parameters. Its dependence on the choice of correlation functions $f_{\mathbf{k}j}(\mathbf{r})$ should be rather weak. In this sense $\xi_{\rm LDA}(\mathbf{p})$ is the universal small correction.

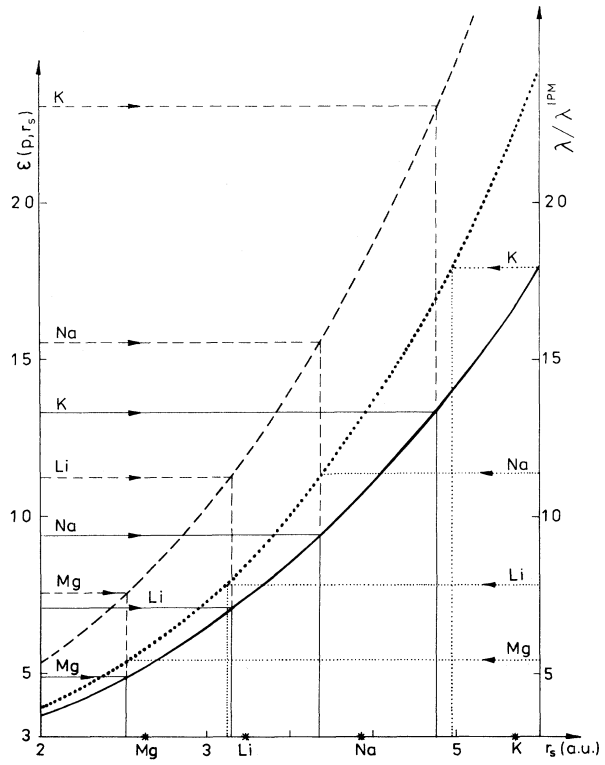

FIG. 3. The effective densities determined by the electron-positron correlation effects (see also Table II). $r_s^{\rm free}$ marked by asterisks are drawn on axis r_s. Values of $\varepsilon^{\rm corr}(0)$ and $\varepsilon^{\rm corr}(p_F)$ [obtained within the LDA (Ref. 11)] are joined with values of the enhancement factors in jellium [Ref. 19(a)], $\varepsilon^{\rm corr}_{\rm jell}(p,r_s)$ for $p=0$ and $p=p_F$ by full and dashed lines, respectively. Dotted line shows correlation function in jellium (Ref. 14) $g(r_s)=\lambda^{\rm jell}/\lambda^{\rm IPM}$ compared with $\gamma=\lambda^{\rm LDA}/\lambda^{\rm IPM}$ for valence electrons (Ref. 15).

In simple metals requirement (i) is well satisfied. The values of $r_s(\mathbf{r}_0)$ and $r_s(\mathbf{r}_1)$ obtained according to Eq. (12) for $\mathbf{p}=\mathbf{0}$ and 1 (in units of $\mathbf{p}_F$), respectively, are shown in Fig. 3 by full and dashed lines. These values are the same providing $r_s^{\rm corr}=r_s(\mathbf{r}_0)=r_s(\mathbf{r}_1)$, listed in column 3 of Table II. The effective density parameters $r_s^{\rm corr}$ differ from the ones characterizing the average valence electron density in the Wigner-Seitz cell, $r_s^{\rm free}$ (columns 2 and 4 of Table II).

It should be noted here that $\varepsilon^{\rm corr}_{\rm jell}(p,r_s)$ is a strongly varying function of density parameter r_s (in the region of metallic and low densities it behaves as r_s^3), while as a function of momentum p it increases at most 60%.[4,9] So, even the considerable relative changes in $\varepsilon^{\rm corr}_{\rm jell}(p,r_s)$ should provide relatively small correction to $r_s^{\rm corr}$ obtained according to Eq. (12). For this reason the function $\zeta(\mathbf{p})$ does not play an important role when the effective density parameters $r_s^{\rm corr}$ are extracted from $\varepsilon^{\rm corr}(\mathbf{p})$ according to Eq. (12). It is not so with relative enhancement factors $\tilde{\varepsilon}(\mathbf{p})=\varepsilon(\mathbf{p})/\varepsilon(\mathbf{0})$ determined by experiment (cf. discussion in I). Its jellium analog $\tilde{\varepsilon}^{\rm corr}_{\rm jell}(p,r_s)=\varepsilon^{\rm corr}_{\rm jell}(p,r_s)/\varepsilon^{\rm corr}_{\rm jell}(0,r_s)$ is weakly dependent on r_s (see Ref. 3 of I) and if we extract $r_s^{\rm corr}$ from relative enhancement factors, the correction $\zeta(\mathbf{p})$ must be taken into account. Since $\zeta(\mathbf{p})$ is universal (it depends only on the structure of material, namely the degree of localization of electrons), we have

$$\tilde{\varepsilon}^{\rm corr}_{\rm LDA}(\mathbf{p})=\tilde{\varepsilon}^{\rm corr}_{\rm AED}(p,r_s^{\rm corr})$$
$$\times\{[1+\zeta_{\rm LDA}(\mathbf{p})]/[1+\zeta_{\rm LDA}(0)]\} \quad (13)$$

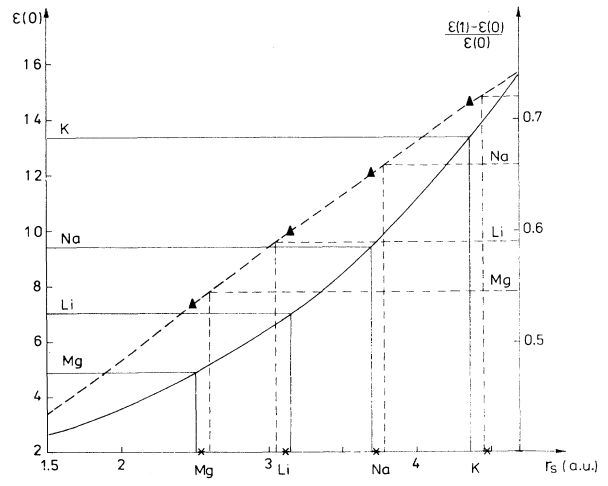

FIG. 4. The same as in Fig. 3 (solid lines and asterisks). Dashed lines and triangles correspond to $r_s^{\rm corr}$, obtained according to Eq. (13) when $\zeta(\mathbf{p})$ is neglected and taken into account, respectively.

TABLE II. The values of the electron density parameters r_s for valence electrons in simple metals. The average valence-electron density parameters r_s^{free} are given in column 2. r_s^{corr} in column 3 denotes the effective densities determined by electron-positron correlations effects basing on $\varepsilon_s^{\text{corr}}(\mathbf{p})$ calculated within the LDA (Ref. 11) for $\mathbf{p}=0$ and $|\mathbf{p}|=|\mathbf{p}_F|$. The relative differences between r_s^{free} and r_s^{corr} are given in column 4. r_s^* in column 5 describes the densities determined by electron-positron correlation effects basing on values of $\gamma^{\text{LDA}}=\lambda_{\text{val}}^{\text{LDA}}/\lambda_{\text{val}}^{\text{IPM}}$ extracted from Ref. 15 (for more details see Fig. 4 and the description in the text).

Metal	r_s^{free}	r_s^{corr}	$\frac{r_s^{\text{corr}}-r_s^{\text{free}}}{r_s^{\text{free}}}$ (%)	r_s^*	$\frac{r_s^{\text{corr}}-r_s^*}{r_s^{\text{corr}}}$ (%)
Be	1.873			1.80	
Al	2.07			2.01	
Mg	2.638	2.53	−4.09	2.53	0.0
Li	3.24	3.15	−2.78	3.12	0.95
Na	3.93	3.70	−5.85	3.72	−0.54
K	4.862	4.40	−9.50	4.47	−1.59
Rb	5.197			4.70	
Cs	6.656			5.04	

The factor $[1+\zeta(\mathbf{p})]/[1+\zeta(0)]$ (listed in Table I) cannot be neglected while determining r_s^{corr} from Eq. (13). In Fig. 4 the values of r_s^{corr} obtained according to Eq. (13) for $p/p_F=1$ when this correction was neglected (dashed line) are compared with those following from including this factor (triangles). It is apparent that if $\zeta(\mathbf{p})$ is taken into account in Eq. (13), the effective electron density parameters are the same as those following from Eq. (12) for absolute enhancement factors. Neglecting $\zeta(\mathbf{p})$ in Eq. (13) for relative enhancement factors $\tilde{\varepsilon}(\mathbf{p})$ (which are the only ones extractable from experiment) may lead to the wrong effective AED, even in simple metals.

The next question is how far r_s^{corr} is universal for the description of the electron-positron correlation effects within AED.[13] The great advantage in studies of the EMD by the positron-annihilation method would be agreement between r_s^{corr} and r_s^* following from total annihilation rates, i.e.,

$$\gamma^{\text{corr}}=\lambda_{\text{val}}/\lambda_{\text{val}}^{\text{IPM}}=\lambda_{\text{jell}}(r_s^*)/\lambda_{\text{jell}}^{\text{IPM}}(r_s^*)=\gamma_{\text{jell}}^{\text{corr}}(r_s^*)\ . \tag{14}$$

The values of r_s^*, obtained according to Eq. (14), where $\gamma_{\text{jell}}^{\text{corr}}(r_s)$ and $\gamma_{\text{val}}^{\text{corr}}$ were taken from Refs. 14 and 15, respectively, are compared with r_s^{corr} in Table II and in Fig. 3. The slight differences between these values (up to 1.5%) should be attributed to the fact that λ_{val} in real metals reads as [cf. Eqs. (4) and (12)]

$$\lambda_{\text{val}}=\int_{\mathbf{p}\in\text{FS}}\varepsilon_{\text{jell}}^{\text{corr}}(p,r_s^{\text{corr}})\rho_{\text{val}}^{\text{IPM}}(\mathbf{p})d\mathbf{p}+\int_{\mathbf{p}\notin\text{FS}}\varepsilon_{\text{jell}}^{\text{corr}}(\mathbf{p})\rho_{\text{val}}^{\text{IPM}}(\mathbf{p})d\mathbf{p}\ .$$

For HMC (the second term) the AED is not applicable (cf. paper I) and the effective electron density is not extractable. Moreover, in electron-gas theories only momenta $p\in\text{FS}$ are considered in expression (4), i.e.,

$$\gamma_{\text{jell}}^{\text{corr}}(r_s)=3\int_{p\in\text{FS}}p^2\varepsilon_{\text{jell}}^{\text{corr}}(p,r_s)dp\ .$$

As the result, the contribution of HMC to λ_{val} may lead to small differences between r_s^* and r_s^{corr} in real metals (especially in K).

V. METHODS OF WORKING WITH COARSE POSITRON EXPERIMENTAL DATA

In the interpretation of experimental ACPAR data, electron-positron enhancement factors are usually approximated according to the biparabolic formula[16]

$$\varepsilon(p)=a+b(p/p_F)^2+c(p/p_F)^4\ . \tag{15}$$

In this section the following problems are discussed:

(i) *Arponen and Pajanne* [Ref. 17(a)]. Measurements in real metals show large variations in the ratio of $(b+c)/a$. The various experimental results, even for simple metals, are not consistent with each other (see Table III).

(ii) *Gustafson and Willenberg* [Ref. 17(b)]. The ratios b/a and c/a vary strongly as the details of the computation procedure are varied and their sum $(b+c)/a$ is a more reliable parameter.

(iii) *Rubaszek and Stachowiak* (Ref. 9). Although the biparabolic Kahana formula (15) is valid for momenta $|\mathbf{p}|\leq 0.8p_F$ (i.e., for about 50% of all electronic states), it is not satisfied near the FS. The parameter $[\varepsilon(p_F)-\varepsilon(0)]/\varepsilon(0)$, which is better defined that b/a and c/a, usually differs from the value of $(b+c)/a$. It is necessary to keep this in mind when one compares experimental data with theoretical predictions.

(iv) *Berko* (Ref. 18). The most important question in the data analysis is how to know the statistical errors of the reconstructed data. If one sees oscillations in $\rho(\mathbf{p})$ (especially for low momenta), does one believe that they are real, that it is a mathematical Fourier transform problem, or that it is error propagation (i.e., noise)?

In the majority of experimental works the coefficients b/a and c/a are determined either from reconstructed densities or from ACPAR [one-dimensional (1D) or two-dimensional (2D)] spectra. Depending on the way of dealing with experimental data, however, the resulting parameters b/a and c/a (as well as their sum) are different (Table III). This disagreement between experimental enhancement factors may be attributed to the fact that the biparabolic approximation (15) is not valid for momenta close to the Fermi momentum. The following

simple test illustrates the problem.

Let us consider the isotropic momentum density $\rho^{2\gamma}(\mathbf{p})=\varepsilon_{\text{jell}}^{\text{corr}}(p,r_s)$ [which differs from (15) near the FS] and calculate the corresponding 1D ACPAR curves

$$N(p_z)=\int\int dp_x dp_y \rho(\mathbf{p})=2\pi\int_{p_z}^{p_F} dp\, p\, \rho^{2\gamma}(p)\ .$$

If we assume that the densities $\rho^{2\gamma}(p)$ can be described by biparabolic formula (15), the corresponding 1D ACPAR spectrum reads as

$$\left\{-p_2^2\left[1+\frac{b}{2}\left[\frac{p}{p_F}\right]^2+\frac{c}{3}\left[\frac{p}{p_F}\right]^4\right]\right\}\ . \tag{16}$$

Of course, in this analysis the experimental error is neglected, while in the interpretation of real data it should be taken into account. The methods of reducing the statistical experimental error are discussed at the end of this section.

Parameters b/a and c/a (and their sum) fitted to curves $\rho^{2\gamma}(p)$ and $N(p_z)$ are given in Table IV (first and second rows, respectively). The values of b/a, c/a, and $(b+c)/a$ depend strongly on the choice of the interpolation points (p_1,p_2,p_3). Moreover, they essentially differ depending on the way of dealing with the data [fitting to $\rho(\mathbf{p})$ or $N(p_z)$; see Table V]. The main reason for these features is the fact that the parabolic formula (15) cannot describe $\rho(p)$ in about 50% of the whole momentum region. This fact is also illustrated in Fig. 5(a), where $\varepsilon(p)$ based on the "reconstructed" density $\rho^{\text{rec}}(p)$ (crosses) and resulting from $N(p_z)$ (solid circles) are compared with $\varepsilon_{\text{jell}}^{\text{corr}}(p,r_s=2)$ (solid line) used in the calculation of both $\rho^{\text{rec}}(p)$ and $N(p_z)$. Figure 6 shows that the reconstruction method [fitting to $\rho(p)$] leads to an appreciably smaller difference between the starting "true" enhancement fac-

TABLE III. Values of the enhancement factors in simple metals determined from 1D or 2D ACPAR spectra. In the last column R and F denote reconstruction and fitting, respectively. Asterisks mark results at 4 kbar pressure and double asterisks show the values of b/a where $\varepsilon=1+(b/a)p^2$ was fitted to ACPAR data. Triple asterisks correspond to reconstructed densities [here $(b+c)/a$ describes the shape of $\varepsilon(\mathbf{p})$ up to $|\mathbf{p}|\le|\mathbf{p}_F|$ only].

Metal	b/a	c/a	$(b+c)/a$	Ref.	Method
Al	0.13	0.12	0.25	6(a)	1D, F^*
	0.1767	0.1282	0.305	6(b), 6(c), 6(e)	1D
	0.132	0.017	0.149	6(d)	2D, F
	0.4		0.4	6(f)	1D, F^{**}
	0.27	0.10	0.37	6(g)	2D, R [100]
	0.25	0.15	0.40	6(g)	[110]
	0.19	0.18	0.37	6(g)	[111]
Mg			0.53±0.19	10(b)	1D, F
	0.20	0.14	0.34±0.03	7(c)	2D, R^{***}
	0.1977	0.1453	0.343	6(e)	1D
	0.7±0.2		0.7±0.2	6(f)	1D, F^{**}
	0.25	0.38	0.63	7(a)	1D, F
	0.20	0.145	0.345	7(b)	1D
	0.18	0.06	0.24	7(d)	2D, R
Li	0.22	0.18	0.40	7(b)	1D
	0.227	0.183	0.41	8(a)	1D
	0.27	0.19	0.46	8(d)	1D, F
	0.20	0.0	0.20	8(f)	2D, F
Na	0.16	0.18	0.34	6(a)	1D, F
	0.60		0.60	6(f)	1D, F^{**}
	0.30	0.27	0.57	8(b)	1D, F
	0.34	0.22	0.56	8(d)	1D, F
	0.0	0.40	0.40	8(f)	2D, F
K	0.9±0.3		0.9±0.3	6(f)	1D, F^{**}
	0.42	0.31	0.73	8(d)	1D, F
	0.3	0.3	0.6	8(e)	1D, F
	0.2	0.4	0.6	8(f)	2D, F
	0.25	0.35	0.6	8(f)	2D, F
Rb	0.46	0.35	0.81	8(d)	1D, F

TABLE IV. The values of parameters b/a and c/a obtained by fitting the electron-gas enhancement factors (for $r_s=6$) to the biparbolic formula (first row). The corresponding parameters fitted to the curves $N(p_z)$ are displayed in the second row. Δ in columns 3, 5, and 7 denotes the relative differences between the values b/a, c/a, and $(b+c)/a$ (shown in columns 2, 4, and 6, respectively) and the average values of corresponding parameters [determined for seven sets of various interpolation points (p_1,p_2,p_3)].

p_1	p_2	p_3	b/a	$\Delta b/a$ (%)	c/a	$\Delta c/a$ (%)	$(b+c)/a$	Δ (%)
0.1	0.5	0.7	0.2084	−1	0.2393	10	0.4477	5
			0.1172	−47	0.4084	10	0.5256	1
0.2	0.5	0.8	0.1962	5	0.2748	−4	0.4710	0
			0.0648	19	0.4635	−2	0.5282	1
0.0	0.5	0.9	0.1959	5	0.3183	−7	0.5142	−9
			0.0108	87	0.5313	−17	0.5420	−2

tor and the fitted one [than fitting ε to $N(p_z)$] for momenta up to $p\cong 0.75p_F$. However, when p approaches the FS, $N(p_z)$ provides a much better fit.

Results shown in Tables IV and V and Figs. 5 and 6 indicate the following.

(i) In the case of fitting to $\varepsilon^{\text{expt}}(p)$ (obtained from reconstructed densities) (a) b/a as well as $(b+c)/a$ (in contrast to c/a) do not depend essentially on the choice of the interpolation points, and (b) up to $p\cong 0.8p_F$ the biparabolic formula describes the momentum dependence of $\varepsilon(p)$ reasonably well and the set of interpolation points (0.2, 0.5, 0.8) seems to provide the best fit (cf. Fig. 6 and Table IV).

(ii) In the case of fitting to $N(p_z)$ (a) $(b+c)/a$ is defined much better than b/a and c/a separately, and (b) the recommended set of interpolation points is (0.1, 0.5, 0.7).

The fact that the sum $(b+c)/a$ is a well-defined parameter does not mean, however, that the interpretation of the experimental results should be limited to the comparison of $(b+c)/a$ with the values of the theoretical enhancement factors at the FS [shown in Fig. 5(b) by the full line]. A much better method is to study the shape of $\rho(p)$ in the whole momentum region, as presented in Fig. 7. If we restrict our analysis to experimental values of $(b+c)/a$, we should compare these quantities with their theoretical analogs given by formulas (15) and (16) (depending on the way of dealing with the data), instead of

TABLE V. The average values of parameters b/a, c/a, and $(b+c)/a$ fitted to $\rho(p)$ and $N(p_z)$ are shown in the first and second rows, respectively. $A(r_s)=[\varepsilon_{\text{jell}}^{\text{corr}}(p_F,r_s)-\varepsilon_{\text{jell}}^{\text{corr}}(0,r_s)]/\varepsilon_{\text{jell}}^{\text{corr}}(0,r_s)$ denotes the values of the relative enhancement factors in jellium at the FS. Δ describe the relative differences between $A(r_s)$ and $(b+c)/a$. $\Delta\varepsilon(p_F)$ is the relative difference between values of $\varepsilon_{\text{jell}}^{\text{corr}}$ and their biparabolic approximation $(b+c)/a$ for $p=p_F$.

r_s	$A(r_s)$	b/a	c/a	$(b+c)/a$	Δ (%)	$\Delta\varepsilon(p_F)$
2	0.56	0.2515	0.1550	0.4065	27	10
		0.1392	0.3255	0.4627	17	6
4	0.629	0.2433	0.2172	0.4604	27	10
		0.1148	0.4103	0.5251	17	6
6	0.629	0.2962	0.2644	0.4706	25	10
		0.0797	0.4527	0.5324	15	6

with $[\varepsilon_{\text{jell}}^{\text{corr}}(1)-\varepsilon_{\text{jell}}^{\text{corr}}(0)]/\varepsilon_{\text{jell}}^{\text{corr}}(0)$ [marked by solid circles or crosses in Fig. 5(b) and given in Table V].

The above results lead to the conclusion that the simultaneous study of reconstructed densities and ACPAR curves $N(p_z)$ could help us answer the question of how far the values of the enhancement factors near the FS differ in real metals from those following from Eq. (15). Since the biparabolic formula (15) does not describe properly $\varepsilon(\mathbf{p})$ near the FS, we propose to correct it in order to reproduce "true" momentum dependence of $\varepsilon(\mathbf{p})$. The corresponding enhancement factor may be written in the form

$$\varepsilon(\mathbf{p})=\varepsilon_b(\mathbf{p})+\varepsilon_c(\mathbf{p})\Theta(0.8\mathbf{p}_F-\mathbf{p}) ,$$

where $\varepsilon_b(p)$ is given by formula (15), Θ is the unit step function, and $\varepsilon_c(\mathbf{p})$ is a correction function. If the enhancement factors $\varepsilon_{\text{jell}}^{\text{corr}}(p)$ following from the ladder approximation to the electron-positron Green's function are considered,[19] the function $\varepsilon_c(p)$ may be approximated in the form

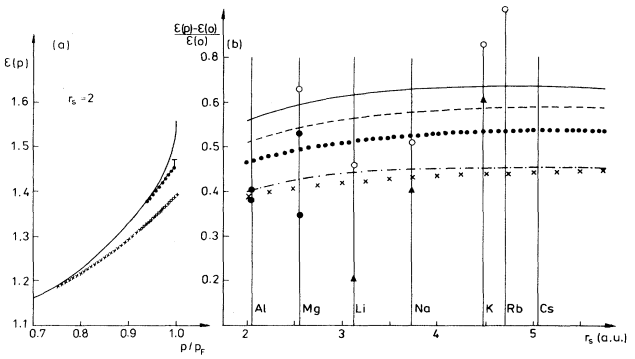

FIG. 5. (a) Values of $\varepsilon_{\text{jell}}^{\text{corr}}(p,r_s)$ in an electron gas for $r_s=2$ (full line) compared with their biparabolic approximation when the parameters b/a and c/a were fitted to $\rho(p)$ (crosses), and to corresponding curve $N(p_z)$ (solid circles). (b) The relative values of $\varepsilon_{\text{jell}}^{\text{corr}}(p,r_s)$ as a function of r_s for $p=p_F$ (full line), $p=0.99p_F$ (dashed line), and $p=0.95p_F$ (dashed-dotted line). $(b+c)/a$ fitted to $\varepsilon^{\text{corr}}(p)$ and $N(p_z)$ are shown by crosses and solid circles, respectively. The experimental values of $(b+c)/a$ are drawn by open circles, triangles, and solid circles (see Table III).

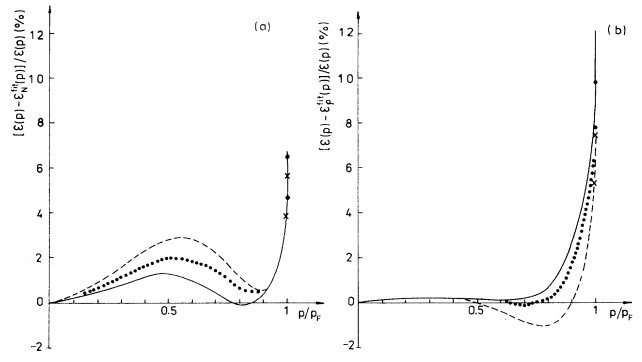

FIG. 6. Relative differences between values of $\varepsilon_{\text{jell}}^{\text{corr}}(p,r_s=2)$ and their biparabolic form $\varepsilon^{\text{fit}}(p)$ for various sets of interpolation points (p_1,p_2,p_3): (0.1, 0.5, 0.7), full line; (0, 0.5, 0.9), dashed line and crosses; and (0.2, 0.5, 0.8), dotted line solid circles . In (a) and (b) the results obtained when the parameters b/a and c/a were fitted to $N(p_z)$ and $\varepsilon(p)$, respectively, are shown.

$$\varepsilon_c(\mathbf{p}/p_F)=d/[1.06-(p/p_F^2)] \quad \text{for } |\mathbf{p}|/p_F \le 1 ,$$

where d is a fitting parameter, dependent on the metal considered. The corresponding 1D ACPAR spectra are equal to

$$N(p_z)=N_b(p_z)+N_c(p_z) ,$$

where $N_b(p_z)$ is given by Eq. (16) and

$$N_c(p_z)=2\pi p_F^2 \int_{p_z/p_F}^{1} p\,\varepsilon_c(p/p_F)dp = \begin{cases} \pi p_F^2 d \ln(7) & \text{for } p_z/p_F \le 0.8 \\ \pi p_F^2 d \ln[(1.06-p_z^2/p_F^2)/0.06] & \text{for } p_z/p_F > 0.8 . \end{cases}$$

The correction $N_c(p_z)$ (which is constant up to $p_z \le 0.8p_F$) amounts to about 2% of $N(p_z=0)$ if $\varepsilon_{\text{jell}}^{\text{corr}}(p,r_s)$ from Ref. 19(b) is applied. Nevertheless, for good experimental statistics, the values of $N_c(p_z)$ are a few times higher than the experimental error (especially for momenta close to $0.8p_F$). The parameter d may be determined from the constant value of $N^{\text{expt}}(p_z)-N_b(p_z)$ in the region $0 \le p \le 0.8p_F$. Investigation of $N_c(p_z)$ for $p > 0.8p_F$ [where $N_c(p_z)$ is a strongly varying function] is not recommended because of experimental errors and smearing of 1D ACPAR data, following from the resolution function of the equipment.

Precise analysis of $N_b(p_z)$ and $N_c(p_z)$ requires first of all correct subtraction of the core contribution. For this purpose the theoretical curves $N^{\text{core}}(p_z)$ should be fitted to experimental ones, $N^{\text{expt}}(p_z)$, for momenta $p_z \ge p_F$. This method seems to be reasonable since recent theoretical results for core contribution to the total annihilation rates[15] give very good agreement with the experimental lifetime measurements. The same occurs for the theoretical enhancement factors for ionic core states, obtained within the LDA.[11(a),15] It is also important to investigate these metals in which HMC not influence visibly the shape of $N^{\text{expt}}(p_z)$. It seems that Na is the most appropriate metal for this analysis. On the other hand, in alkali metals the Fermi momentum is rather small and the influence of the resolution function of the equipment can unable us to study $\rho^{\text{rec}}(\mathbf{p})$ and $N^{\text{expt}}(p_z)$ in the neighborhood of $0.8p_F$. As a conclusion, detailed studies of $N_c(p_z)$ require the equipment of high resolution, such as the one used by Kubica and Stewart.[7(a)]

Reconstruction techniques for 1D and 2D ACPAR data were described by Pecora,[20] who discussed momentum- and Fourier-space spherical harmonics reconstruction methods. The alternative approaches have been proposed by Cormack[21] and Reiter and Silver:[22] the expansion of measured projections into a set of orthogonal polynomials. The resulting densities $\rho(\mathbf{p})$ are sums of the corresponding orthogonal polynomials. If planar projections of $\rho(\mathbf{p})$ (1D data) are expanded in terms of Hermitian polynomials and spherical harmonics, densities $\rho(\mathbf{p})$ are given as a series of the Laguerrian polynomials and spherical harmonics. For linear projections of $\rho(\mathbf{p})$ (2D data) application of Chebyshev polynomials of the second kind [with the weight function $(1-p^2)^{1/2}$] gives $\rho(\mathbf{p})$ as a series of Zernike polynomials. We recommend techniques of Refs. 21 and 22 for the following reasons.[21,23]

(i) The expansion of experimental data into orthogonal

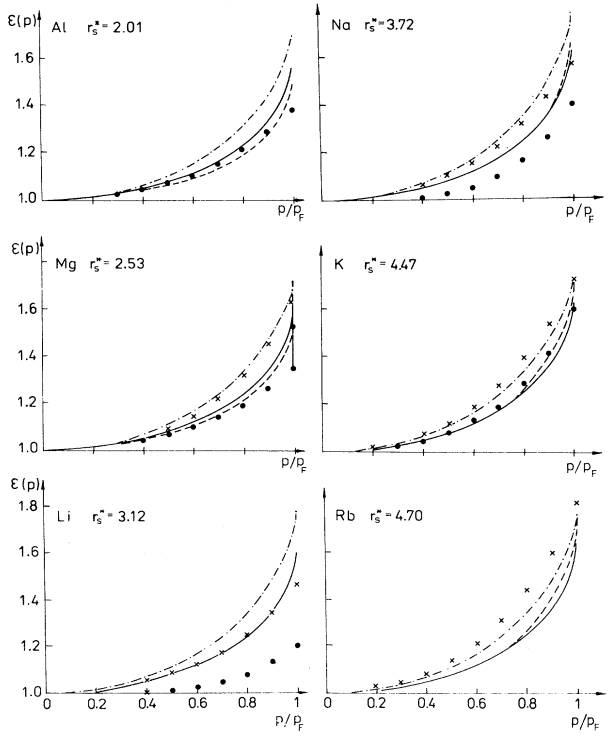

FIG. 7. Enhancement factors $\varepsilon_{\text{jell}}^{\text{corr}}(p,r_s)$ following from various electron-gas theories (full [Ref. 19(a)], dashed [Ref. 19(b)], and dash-dotted [Ref. 19(c)] lines) compared with "experimental" enhancement factors given in Table III. Crosses show results of Ref. 8(d) and solid circles (Li, Na, and K) are results by Oberli *et al.* [Ref. 8(f)]. For Al and Mg the reconstructed densities from Refs. 6(g) and 7(c), respectively, are presented.

polynomials shares the least-squares approximation properties of these functions and hence properly takes experimental errors into account.

(ii) Measured projections are dependent on each other as they represent integrals of the same density. The so-called "consistency condition" for 2D data was discussed in Ref. 23. It was shown that this condition suppresses the noise in the data making additional advantage of the method.

Of course, in order to reproduce the shape of anisotropic density $\rho(\mathbf{p})$ properly, the best way is to perform a reconstruction of 2D ACPAR spectra. However, in order to determine the true shape of $\varepsilon(\mathbf{p})$ or $\rho(\mathbf{p})$ the analysis of 1D ACPAR curves seems to be more reliable. In this connection we limit our consideration to 1D ACPAR spectra.

The only quantity which can be estimated exactly from $N(p_z)$ is the isotropic component of the density $\rho^0(p)$. $\rho^0(p)$ describes the true isotropic component of $\rho^{\text{expt}}(\mathbf{p})$ only in the case when $N(p_z)$ are almost isotropic (nearly isotropic FS as well as small contribution of HMC). The isotropic component of 1D data, $g_0(p)$, is given by the relation[24]

$$N_{\beta,\alpha}(p)=g_0(p)+\sum_{l,\nu} g_{l,\nu}(p)K_{l,\nu}(\beta,\alpha) , \tag{17}$$

where $K_{l,\nu}$ are the spherical harmonics and angles (β,α) describe the orientation of p_z with respect to the crystal axis. Knowledge of $g_0(p)$ enables us to calculate $\rho^0(p)$ from the relation[25]

$$\rho_0(p)=-\frac{1}{p}\frac{dg_0(p)}{dp} . \tag{18}$$

However, the calculation of the derivative of $g_0(p)$ in Eq. (18) is troublesome because $g_0(p)$ is very sensitive to the experimental errors. In the case of 1D ACPAR data, the expansion of $g_0(p)$ into the Chebyshev polynomials of the first kind

$$g_0(p)=\sum_{m=0}^{N} a_m T_{2m}(p) \tag{19}$$

seems to be the most favorable because it allows us to reduce the statistical experimental error in the highest degree. Due to orthogonality of $T_k(x)$, the coefficients a_m may be written as[26]

$$a_m=\frac{4}{\pi}\int_0^1 (1-p^2)^{-1/2} g_0(p)T_{2m}(p)dp .$$

In the unit system $p=\cos(t)$, a_m reads as

$$a_m=\frac{4}{\pi}\int_0^{\pi/2} g_0(\cos t)\cos(2mt)dt .$$

According to Eqs. (18) and (19), the isotropic component $\rho^0(p)$ is given by

$$\rho^0(p)=-\frac{1}{p\pi}\sum_{m=1}^{N} m a_m U_{2m-1}(p) , \tag{20}$$

where $U_m(p)$ are the Chebyshev polynomials of the second kind. In the limit p equal to zero,

$$\rho^0(p=0)=-2a_1/\pi .$$

This procedure, allowing us to reduce the experimental errors as well as to draw the shape of $\rho^0(p)$ with high accuracy, is to be described in more details elsewhere.[27] The expansion of the experimental data into series (19) allows us to reproduce the shape of the experimental curve $g_0(p)$ in detail. The calculation of $\rho^0(p)$ for various numbers of the expansion coefficients enables us to reproduce the shape of the density with high precision. This analysis allows us to answer the question of which oscillations in $\rho(\mathbf{p})$ are real and which are due to the errors propagation. In contrast to this method, smoothing of the experimental curves (e.g., by Spline function) in order to eliminate the statistical error causes the smearing of $N(p_z)$ [and corresponding $\rho^{\text{expt}}(\mathbf{p})$] at the FS.

VI. CONCLUSIONS

Band-structure calculations results indicate that, for NFE populations (e.g., valence electrons in simple metals), neither the positron distribution nor local state-independent electron-positron correlations can change visibly momentum density of annihilation pairs with respect to the EMD. The slight jumps of $\rho^{2\gamma}(\mathbf{p})$ observed in the region of bands superposition are mainly due to the deviation of $\rho^e(\mathbf{p})$ from the step function, i.e., to the band effects. These results confirm our general considerations presented in I. Moreover, $\rho_0^{2\gamma}(\mathbf{p})$ and $\rho^{\text{IPM}}(\mathbf{p})$ are closer to the step function than $\rho^e(\mathbf{p})$ (except Li). This fact suggests that the positron distribution reduces band effects in $\rho^{2\gamma}(\mathbf{p})$.

The AED works for valence electrons in simple metals reasonably well for momenta $\mathbf{p}$ inside the FS. The correlation effects may be described quite correctly within the jellium model if only the proper electron density is taken into account. Knowledge of the effective density allows for verification of electron-gas theory before applying it to the calculation of annihilation characteristics in more complicated metals with the LDA. Without a doubt effective electron densities differ from average valence electron densities in the Wigner-Seitz cell, r_s^{free}. This fact should be taken into account when the electron-gas theory results are compared with experimental data.

Applicability of AED enables us to avoid performing laborious calculations of convolutions of electron and positron wave functions with local electron-positron correlation function. Knowing the values given in Table I we can restrict our calculations of $\rho^{2\gamma}(\mathbf{p})$ to $\rho^e(\mathbf{p})$.

In the majority of experimental works the real form of the enhancement factor $\varepsilon_{\text{expt}}^{\text{corr}}(\mathbf{p})$ is approximated by the biparabolic formula which is not valid near the FS even for such a simple model as an electron gas. This fact may be the main reason for a lack of consistency between various experimental results for b/a, c/a, and $(b+c)/a$, even in simple metals. The values of these parameters extracted from experimental curves strongly depend on the way of dealing with the data and fitting procedure. Only a simultaneous analysis of $\rho^{\text{rec}}(\mathbf{p})$ and 1D ACPAR data (described in Sec. V) could enable us to determine the momentum dependence of $\varepsilon(\mathbf{p})$ near the FS.

In order to diminish the influence of experimental errors on the results, the expansion of 1D ACPAR data into a series of orthonormal Chebyshev polynomials of the first kind is proposed. This expansion has the least-squares approximation properties and hence properly takes experimental errors into account. As a result, the isotropic component of the momentum density is given as a series of Chebyshev polynomials of the second kind. This allows us to determine the values of the density $\rho^0(\mathbf{p})$ with high accuracy in the whole momentum region, even for momentum p equal to zero.

ACKNOWLEDGMENTS

We are grateful to Dr. J. Majsnerowski for the numerical values listed in Table I, kindly made accessible. Work is supported by the State Committee for Scientific Research under Grant No. 2 0307 91 01.

[1]G. Kontrym-Sznajd and A. Rubaszek, preceding paper, Phys. Rev. B **47**, 6950 (1993).

[2]S. Daniuk, G. Kontrym-Sznajd, J. Mayers, A. Rubaszek, H. Stachowiak, P. A. Walters, and R. N. West, J. Phys. F **17**, 1365 (1987).

[3]B. Chakraborty, Phys. Rev. B **24**, 7423 (1981).

[4]For a review see Ref. 1.

[5]References 6–8 are devoted to experimental momentum-dependent enhancement factors in simple metals: Al (Ref. 6), Mg [Refs. 6(f) and 7], and alkali metals [Refs. 6(a), 6(f), 7(b), and 8].

[6](a) D. R. Gustafson and J. D. Willenberg, Phys. Rev. B **13**, 5193 (1976); (b) T. Okada, H. Sekizawa, and N. Shiotani, J. Phys. Soc. Jpn. **41**, 836 (1976); (c) J. Mader, S. Berko, H. Krakauer, and A. Bansil, Phys. Rev. Lett. **37**, 1232 (1976); (d) A. A. Manuel, S. Samoilov, O. Fisher, and M. Peter, Helv. Phys. Acta **52**, 255 (1979); in *Positron Annihilation,* edited by R. R. Hasiguti and K. Fujiwara (Japanese Institute of Metals, Senedai, 1979), p. 685; (e) N. Shiotani, T Okada, H. Sekizawa, and S. Wakoh, J. Phys. Soc. Jpn. **50**, 498 (1981); (f) P. Kubica and A. T. Stewart, Can. J. Phys. **61**, 971 (1983); (g) H. Nakashima, T. Kubota, Y. Murakami, H. Kondo, and S. Tanigawa, in *Positron Annihilation,* Vols. 105–110 of *Materials Science Forum,* edited by Zs. Kajcsos and Cs. Szeles (Trans Tech, Aedermannsdorf, Switzerland, 1992), p. 779.

[7](a) P. Kubica and A. T. Stewart, Phys. Rev. Lett. **34**, 852 (1975); (b) P. Kubica, B. T. McKee, A. T. Stewart, and M. J. Stott, Phys. Rev. B **11**, 11 (1975); (c) cf. Ref. 11(c), where the reconstructed densities are based on the experimental data by P. A. Walters, J. Mayers, and R. N. West, in *Positron Annihilation,* edited by P. G. Coleman, S. C. Sharma, and L. M. Diana (North-Holland, Amsterdam, 1982), p, 334; (d) H. Nakashima, T. Kubota, H. Kondo, and S. Tanigawa, in *Positron Annihilation* [Ref. 6(g)], p. 771.

[8](a) J. Melngailis and S. DeBenedetti, Phys Rev. **145**, 400 (1966); (b) J. J. Donaghy and A. T. Stewart, *ibid.* **164**, 396 (1967); (c) J. A. Arias-Limonta and P. G. Varlashkin Phys. Rev. B **1**, 142 (1970); (d) S. M. Kim and A. T. Stewart, *ibid.* **11**, 2490 (1975); (e) T. Hyodo, T. McMullen, and A. T. Stewart, in *Positron Annihilation* [Ref. 7(c)], p. 201; (f) L. Oberli, A. A. Manuel, A. K. Singh, T. Jarlborg, L. P. L. M. Rabou, P. E. Mijnarens, T. Hyodo, and A. T. Stewart, in *Positron Annihilation,* edited by P. C. Jain, R. M. Singru, and K. P. Gopinathan (World Scientific, Singapore, 1985), p. 251.

[9]A. Rubaszek and H. Stachowiak, J. Phys. F **15**, L231 (1985).

[10](a) In the case of approach developed in Ref. 10(b) p_0 is chosen close to $0.8p_F$. Theory of Ref. 10(c) seems to choose $p_0=0$ (the same as that which concerns positron annihilation with ionic cores [Ref. 11(a)]); (b) J. Arponen, P. Hautojäroi, R. Nieminen, and E. Pajanne, J. Phys. F **3**, 2092 (1973); (c) T. Jarlborg and A. K. Singh, Phys. Rev. B **37**, 4460 (1987).

[11](a) S. Daniuk, G. Kontrym-Sznajd, J. Majsnerowski, M. Sob, and H. Stachowiak, J. Phys. Condens. Matter **1**, 6321 (1989); see in *Positron Annihilation* [Ref. 6(g)], p. 627; (b) J. Majsnerowski, Ph.D. thesis, Institute of Low Temperatures and Structure Research, Wrocław, 1990; (c) G. Kontrym-Sznajd and J. Majsnerowki, J. Phys.: Condens Matter **2**, 9927 (1990).

[12]H. Sormann, Phys. Rev. B **43**, 8841 (1991).

[13]G. Kontrym-Sznajd and S. Daniuk, see in *Positron Annihilation* [Ref. 6(g)], p. 695

[14]E. Boronski and Nieminen, Phys. Rev. B **34**, 3820 (1988).

[15]S. Daniuk, M. Sob, and A. Rubaszek, Phys. Rev. B **43**, 2580 (1991).

[16]S. Kahana, Phys. Rev. **129**, 1622 (1963).

[17](a) J. Arponen and E. Pajanne, J. Phys. F **9**, 2359 (1979); (b) D. R. Gustafson and J. D. Willenberg, Phys. Rev. B **13**, 5193 (1976).

[18]There is an open discussion on experimental techniques and data analysis at ICPA 8, in *Positron Annihilation,* edited by L. Dorikens-Vanpraet, M. Dorikens, and D. Segers (World Scientific, Singapore, 1988), p. 216.

[19](a) A. Rubaszek and H. Stachowiak, Phys. Rev. B **38**, 3846 (1988); (b) Phys. Status Solidi B **124**, 159 (1984); (c) H. Stachowiak, Phys. Rev. B **41**, 12 522 (1990).

[20]L. M. Pecora, J. Phys.: Condens. Matter **1**, SA1 (1989).

[21]A. M. Cormack, J. Appl. Phys. **35**, 2908 (1964); Phys. Med. Biol. **18**, 195 (1983).

[22]G. Reiter and R. Silver, Phys. Rev. Lett. **54**, 1047 (1985).

[23]G. Kontrym-Sznajd, Phys. Status Solidi A **117**, 227 (1990); see in *Positron Annihilation* [Ref. 6(g)], p. 325.

[24]P. E. Mijnarends, Phys. Rev. **178**, 622 (1969).

[25]A. T. Stewart, Can. J. Phys. **35**, 168 (1957).

[26]S. Paszkowski, *Numerical Application of Chebyshev Polynomials and Series* (Polish Scientific, Warsaw, 1975) (in Polish).

[27]G. Kontrym-Sznajd (unpublished).